

Electronic Supplementary Information

Tuning electrical properties of phenanthroimidazole derivatives to construct multifunctional deep-blue electroluminescent materials

Ze-Lin Zhu,^{a,b} Shao-Fei Ni,^c Wen-Cheng Chen,^a Miao Chen,^d Jie-Ji Zhu,^d Yi Yuan,^e Qing-Xiao Tong,^{d*} Fu-Lung Wong,^a and Chun-Sing Lee^{a,b*}

^a Center of Super-Diamond and Advanced Films (COSDAF) & Department of Chemistry, City University of Hong Kong, Hong Kong SAR, PR China. E-mail: apcslee@cityu.edu.hk

^b City University of Hong Kong Shenzhen Research Institute, 8 Yuexing 1st Road, Shenzhen Hi-Tech Industrial Park, Nanshan District, Shenzhen 518000, China

^c Department of Chemistry, South University of Science and Technology of China, Shenzhen, 518055, P.R. China

^d Department of Chemistry and Key Laboratory for Preparation and Application of Ordered Structural Materials of Guangdong Province, Shantou University, 243 University Road, Shantou, Guangdong, 515063, PR China. E-mail: qxtong@stu.edu.cn

^e Jiangsu Key Laboratory for Carbon-Based Functional Materials & Devices, Institute of Functional Nano & Soft Materials (FUNSOM) & Collaborative Innovation Center of Suzhou Nano Science and Technology, Soochow University, Suzhou, 215123, PR China.

Synthesis

4'-(diphenylamino)-[1,1'-biphenyl]-4-carbaldehyde

In toluene (30 mL), (4-(diphenylamino)phenyl)boronic acid (1.73 g, 6 mmol), 4-bromobenzaldehyde (1.22 g, 6.6 mmol), Pd(PPh₃)₄ (0.35 g, 0.03 mmol), K₂CO₃ aqueous (2 M, 9 mL) and ethanol (6 mL) were added and refluxed in an argon atmosphere for 24 h. The solution was cooled to room temperature and extracted with CH₂Cl₂. The extract was dried with anhydrous Na₂SO₄ and concentrated by rotary evaporation. The residue was purified by column chromatography (eluent: petroleum ether/CH₂Cl₂ = 4/1) to obtain the pure product as white powder. Yield: 88%.

4'-(1-(4-bromophenyl)-1*H*-phenanthro[9,10-*d*]imidazol-2-yl)-*N,N*-diphenyl-[1,1'-biphenyl]-4-amine

The 4'-(diphenylamino)-[1,1'-biphenyl]-4-carbaldehyde (1.75 g, 5 mmol), 9,10-phenanthrenequinone (1.04 g, 5 mmol), 4-bromoaniline (0.86 g, 5 mmol), and ammonium acetate (1.54 g, 20.0 mmol) were refluxed in an acetic acid solution under an argon atmosphere for 3 h. After cooling to room temperature, an orange-yellow mixture was obtained and poured into methanol under stirring. The raw product was separated by filtration and washed with methanol, and then dried under vacuum. The product was purified by column chromatography (eluent: petroleum ether/CH₂Cl₂ = 2/1) to give a white powder Yield 91%.

(4-(2-(4'-(diphenylamino)-[1,1'-biphenyl]-4-yl)-1*H*-phenanthro[9,10-*d*]imidazol-1-yl)phenyl)diphenylphosphine oxide (TPAPOPPI)

To a mixture of NiCl₂·6H₂O (0.28g, 1.2 mmol), zinc (1.6 g, 24.0 mmol), 2,2-bipyridine (bpy) (0.36 g, 2.4 mmol) and 4'-(1-(4-bromophenyl)-1*H*-phenanthro[9,10-*d*]imidazol-2-yl)-*N,N*-diphenyl-[1,1'-biphenyl]-4-amine (2.77 g, 4 mmol) in DMAc (40.0 ml) solution, biphenylphosphine oxide (1.6 g, 8.0 mmol) was added. The reaction mixture was magnetically stirred at 110 °C for 24 hours and then allowed to cool to room temperature. The solution was filtrated and 250 ml CH₂Cl₂ was added. After wash with water 5 times, the solvent was removed by rotary evaporation. The target product was purified by column chromatography (eluent: ethyl acetate/CH₂Cl₂ = 1/500). Yield 70.5%. ¹H NMR (400 MHz, Methylene Chloride-*d*₂) δ 8.84 (d, *J* = 8.3 Hz, 1H), 8.78 (d, *J* = 8.3 Hz, 1H), 7.99 – 7.91 (m, 2H), 7.88 (d, *J* = 8.4 Hz, 1H), 7.84 – 7.50 (m, 20H), 7.40 – 7.31 (m, 5H), 7.31 – 7.27 (m, 1H), 7.24 – 7.15 (m, 7H), 7.15 – 7.08 (m, 2H).; MS (ESI) *m/z*: [M + H]⁺ calcd for C₅₇H₄₀N₃OP, 813.92; found, 814.21.

4-(9-phenyl-9*H*-carbazol-3-yl)benzaldehyde

Reaction and purification conditions were the same as for 4'-(diphenylamino)-[1,1'-biphenyl]-4-carbaldehyde, except (9-phenyl-9*H*-carbazol-3-yl)boronic acid (1.72 g, 6 mmol) was used. Yield 85.3%.

1-(4-bromophenyl)-2-(4-(9-phenyl-9*H*-carbazol-3-yl)phenyl)-1*H*-phenanthro[9,10-*d*]imidazole

Reaction and purification conditions were the same as for 4'-(1-(4-bromophenyl)-1*H*-phenanthro[9,10-*d*]imidazol-2-yl)-*N,N*-diphenyl-[1,1'-biphenyl]-4-amine, except 4-(9-phenyl-9*H*-carbazol-3-yl)benzaldehyde (1.74 g, 5 mmol) was used. Yield 86.6%.

diphenyl(4-(2-(4-(9-phenyl-9*H*-carbazol-3-yl)phenyl)-1*H*-phenanthro[9,10-*d*]imidazol-1-yl)phenyl)phosphine oxide (3-CzPOPPI)

Reaction and purification conditions were the same as for **TPAPOPPI**, except 1-(4-bromophenyl)-2-(4-(9-phenyl-9*H*-carbazol-3-yl)phenyl)-1*H*-phenanthro[9,10-*d*]imidazole (2.76 g, 4 mmol) was used. Yield 40.9 %. ¹H NMR (400 MHz, Methylene Chloride-*d*₂) δ 8.86 (d, *J* = 8.4 Hz, 1H), 8.80 (d, *J* = 8.3 Hz, 1H), 8.46 (d, *J* = 1.8 Hz, 1H), 8.26 (dt, *J* = 7.7, 1.1 Hz, 1H), 7.99 (dd, *J* = 11.2, 8.1 Hz, 2H), 7.84 (t, *J* = 7.4 Hz, 2H), 7.81 – 7.72 (m, 12H), 7.72 – 7.62 (m, 7H), 7.62 – 7.54 (m, 6H), 7.50 (dd, *J* = 3.6, 1.1 Hz, 2H), 7.38 (ddd, *J* = 8.1, 5.0, 3.2 Hz, 2H), 7.30 (d, *J* = 8.3 Hz, 1H). MS (ESI) *m/z*: [M + H]⁺ calcd for C₅₇H₃₈N₃OP, 811.90; found, 812.6.

4'-(9*H*-carbazol-9-yl)-[1,1'-biphenyl]-4-carbaldehyde

Reaction and purification conditions were the same as for 4'-(diphenylamino)-[1,1'-biphenyl]-4-carbaldehyde, except (4-(9*H*-carbazol-9-yl)phenyl)boronic acid (1.72 g, 6 mmol) was used. Yield 80.4%.

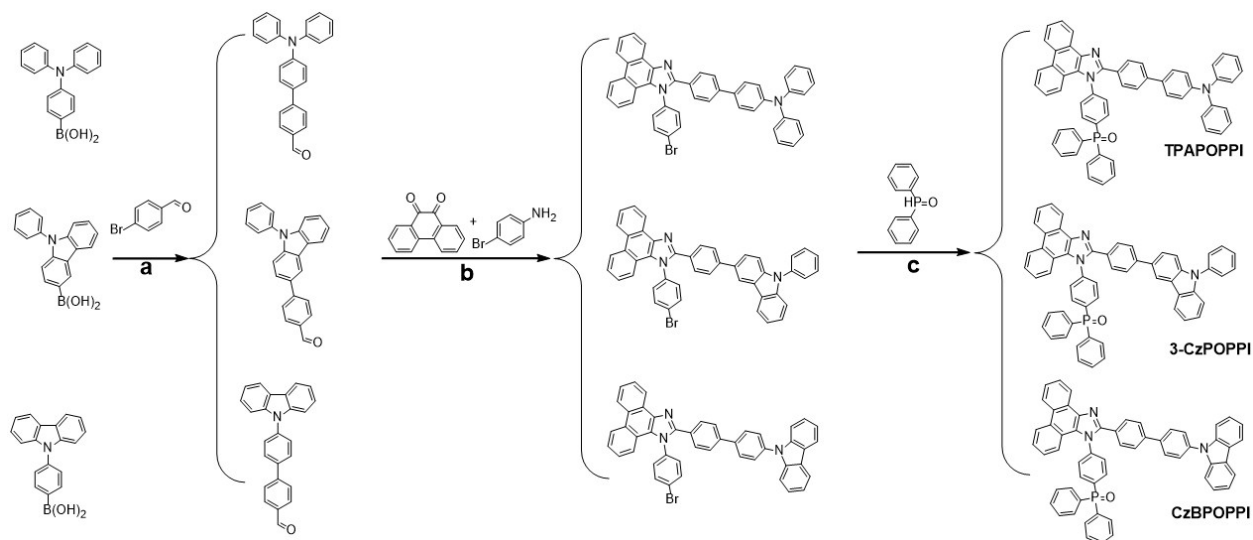
2-(4'-(9*H*-carbazol-9-yl)-[1,1'-biphenyl]-4-yl)-1-(4-bromophenyl)-1*H*-phenanthro[9,10-*d*]imidazole

Reaction and purification conditions were the same as for 4'-(1-(4-bromophenyl)-1*H*-phenanthro[9,10-*d*]imidazol-2-yl)-*N,N*-diphenyl-[1,1'-biphenyl]-4-amine, except 4'-(9*H*-carbazol-9-yl)-[1,1'-biphenyl]-4-carbaldehyde (1.74 g, 5 mmol) was used. Yield 79.6%.

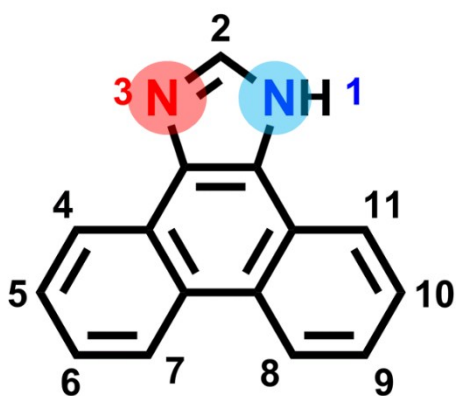
(4-(2-(4'-(9*H*-carbazol-9-yl)-[1,1'-biphenyl]-4-yl)-1*H*-phenanthro[9,10-*d*]imidazol-1-yl)phenyl)diphenylphosphine oxide (CzBPOPPI)

Reaction and purification conditions were the same as for **TPAPOPPI**, except 2-(4'-(9*H*-carbazol-9-yl)-[1,1'-biphenyl]-4-yl)-1-(4-bromophenyl)-1*H*-phenanthro[9,10-*d*]imidazole (2.76 g, 4 mmol) was used. Yield 60 %. ¹H NMR (400 MHz, Methylene Chloride-*d*₂) δ 8.87 (d, *J* = 8.4 Hz, 1H), 8.81 (d, *J* = 8.3 Hz,

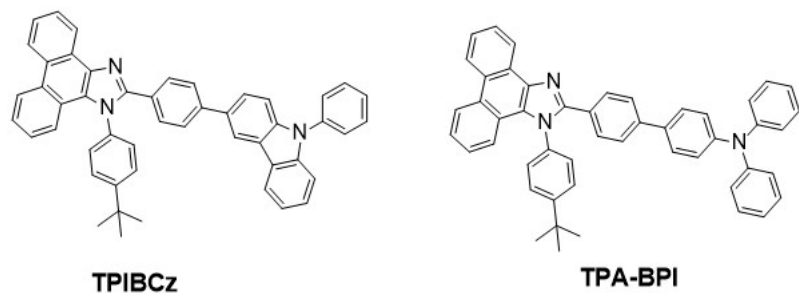
1H), 8.22 (dt, $J = 7.7, 1.0$ Hz, 2H), 8.00 (dd, $J = 11.3, 8.0$ Hz, 2H), 7.95 – 7.89 (m, 2H), 7.85 (t, $J = 7.5$ Hz, 2H), 7.77 (tdd, $J = 8.4, 4.3, 2.3$ Hz, 12H), 7.71 – 7.64 (m, 3H), 7.63 – 7.47 (m, 9H), 7.43 – 7.33 (m, 3H), 7.32 – 7.27 (m, 1H). MS (ESI) m/z : $[M + H]^+$ calcd for $C_{57}H_{38}N_3OP$, 811.90; found, 812.25.



Scheme S1. Synthetic routes of the new compounds. a: $2M K_2CO_3$, $Pd(PPh_3)_4$, toluene, EtOH, $90^\circ C$; b: AcOH, AcONH₄, $120^\circ C$; c: $NiCl_2 \cdot 6H_2O$, Zn, bpy, DMAc, $110^\circ C$



Scheme S2. Atom position of phenanthroimidazole in chemical nomenclature.



Scheme S3. Chemical structure of TPIBCz and TPA-BPI.

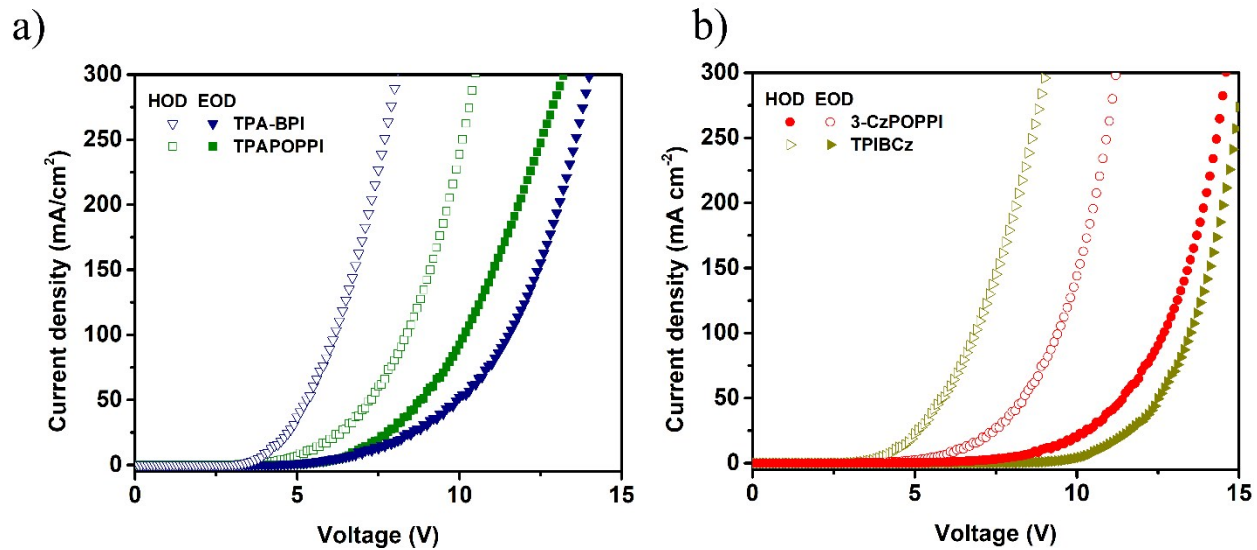


Fig. S1. Current density-voltage characteristics of the electron- and the hole-only devices of a) TPAOPPI and TPA-BPI; b) 3-CzPOPPI and TPIBCz.

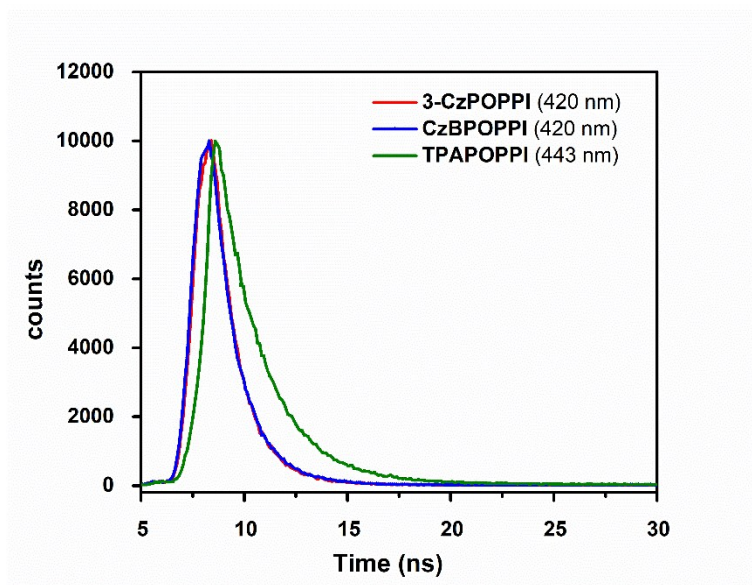


Fig. S2 Time-dependent PL measurement of the new emitters in DCM (the number in the bracket is the emission wavelength detected).

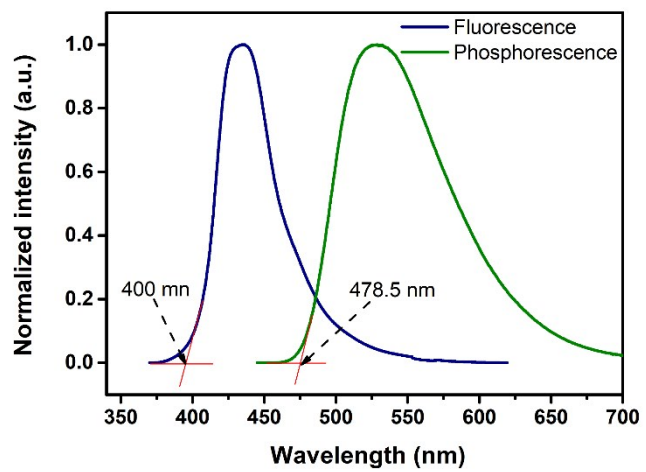


Fig. S3 Low temperature (77 K) fluorescence and phosphorescence spectrum of **TPAPOPPI** in 2-Me-THF

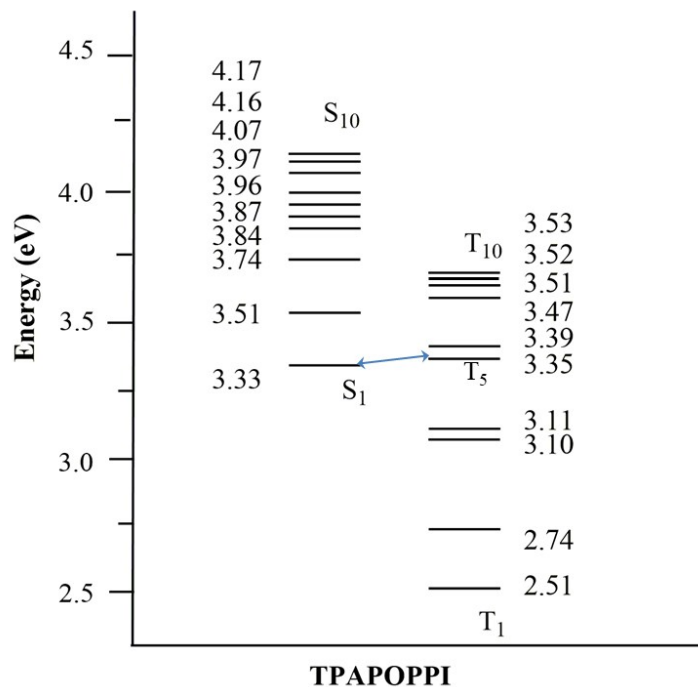


Fig. S5 Energy diagram of the first ten excited states of TPAPOPPI (the blue arrow represents the possible reverse intersystem crossing pathway).

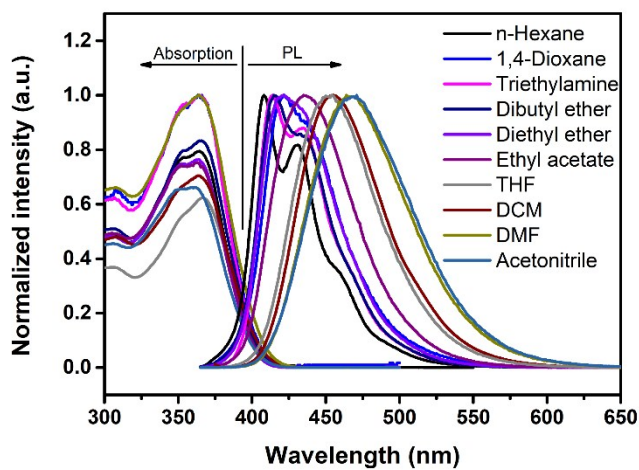


Fig. S6 Solvent-dependent absorption and PL spectra of TPAPOPPI.

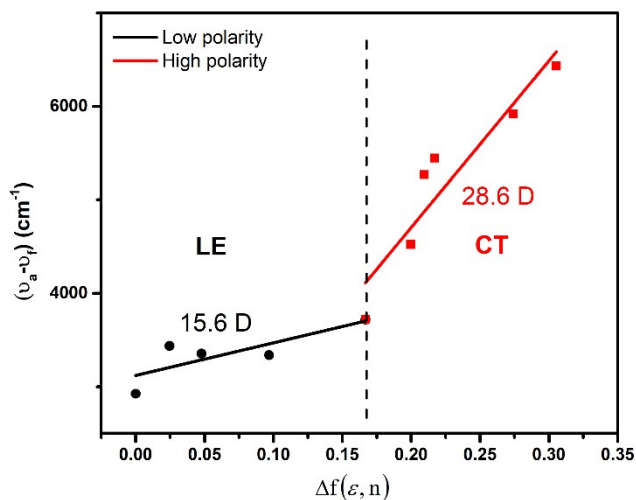


Fig. S7 linear fitting based on the Lippert-Mataga model in various solvents.

Table S1. Solvatochromic UV-PL data for Lippert-Mataga model

solvents	TPAPOPPI			
	$\Delta f(\epsilon, n)$	λ_a (nm)	λ_f (nm)	$\nu_a - \nu_f$ (cm ⁻¹)
n-Hexane	0	364.5	408	2925.038
1,4-Dioxane	0.024512	367	420	3438.433
Triethylamine	0.047682	363.5	414	3355.727
Dibutyl ether	0.096823	364.5	415	3338.457
Diethyl ether	0.166749	364	421	3719.558
Ethyl acetate	0.199635	363.5	435	4521.811
Tetrahydrofuran	0.209572	367	455	5269.934
Dichloromethane	0.217137	364	454	5446.096
N,N-Dimethylformamide	0.27438	364	464	5920.803
Acetonitrile	0.305416	361.5	471	6431.095

The Lippert-Mataga model is estimated according to literatures.^{1,2}

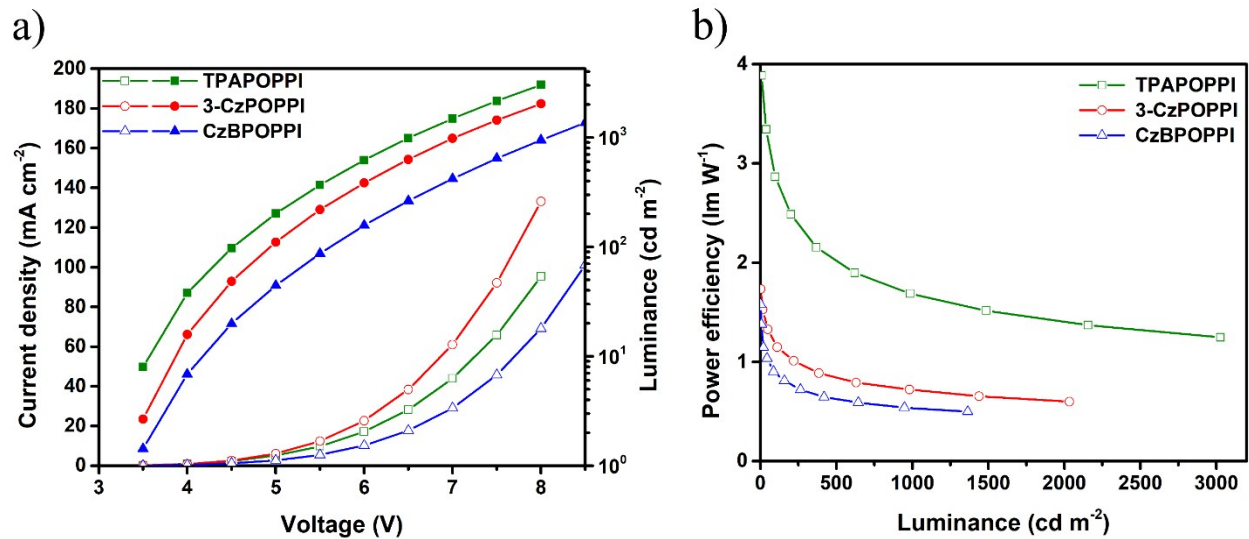


Fig. S8 a) Current density-voltage-luminescence characteristic curves and b) plots of power efficiency luminance of the doped device.

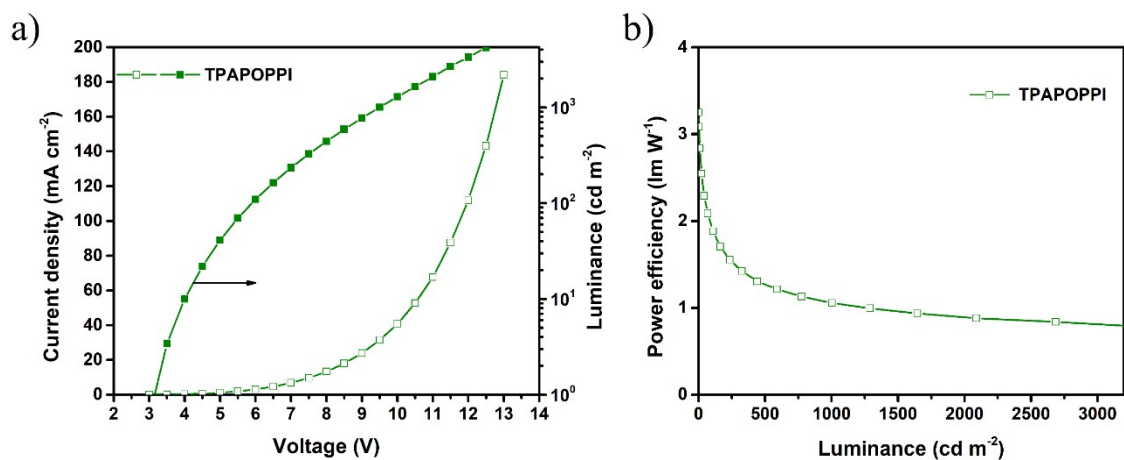


Fig. S9 a) Current density-voltage-luminescence characteristic curves and b) plots of power efficiency luminance of the single layer device.

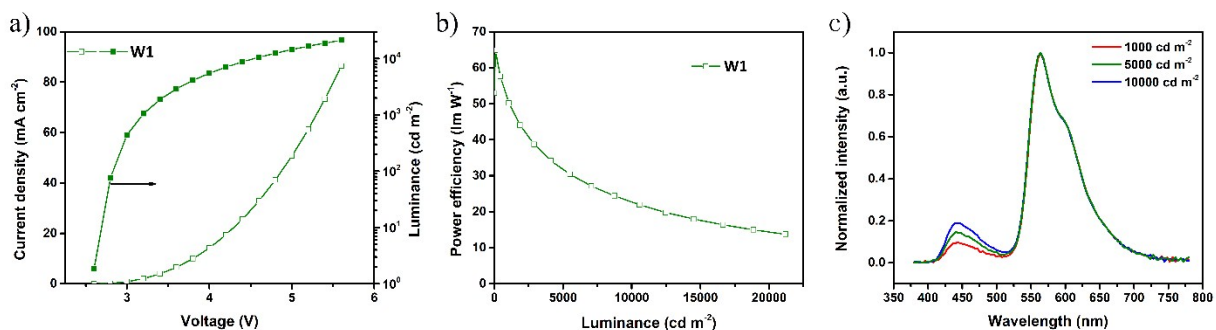


Fig. S10 a) Current density-voltage-luminescence characteristic curves, b) plots of power efficiency-luminance and c) EL spectra at 1,000, 5,000 and 10,000 cd m^{-2} of device W1.

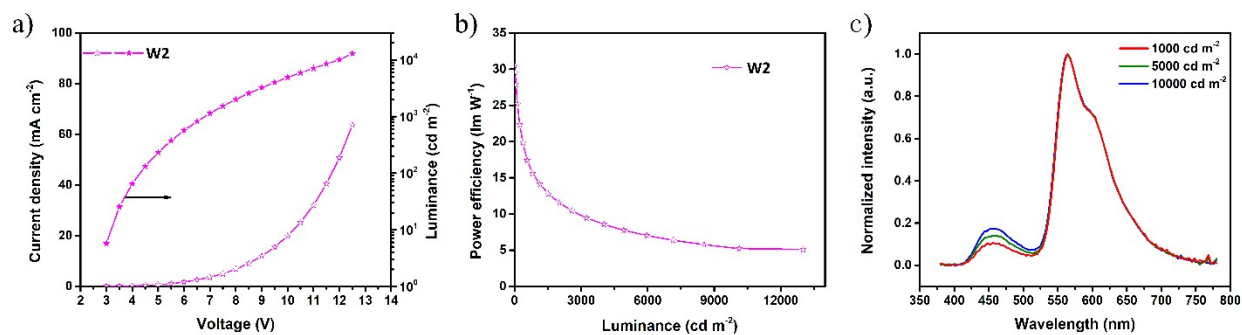


Fig. S11 a) Current density-voltage-luminescence characteristic curves, b) plots of power efficiency-luminance and c) EL spectra at 1,000, 5,000 and 10,000 cd m⁻² of device W2.

Notes and references

- 1 P. Suppan, *Chem. Phys. Lett.*, 1983, **94**, 272–275.
- 2 S. Zhang, L. Yao, Q. Peng, W. Li, Y. Pan, R. Xiao, Y. Gao, C. Gu, Z. Wang and P. Lu, *Adv. Funct. Mater.*, 2015, **25**, 1755–1762.